Supplementary Information (SI) for ChemComm.
This journal is © The Royal Society of Chemistry 2026

Supplementary Information

Multi-Functional Polymer Coating Enabling Stable Zn Anodes for High Performance Zinc-Ion Batteries

Characterization details

Materials Characterizations

The material morphologies were characterized using scanning electron microscopy (SEM, HITACHI SU8010, Japan) and transmission electron microscopy (TEM, FEI Talos F200X, USA). The crystal phases were identified through X-ray diffraction (XRD, Bruker D8 Advance, Holland) with Cu Kα radiation (λ = 0.154 nm). Chemical structures and surface compositions were further analyzed by Fourier transform infrared spectroscopy (FT-IR, Nexus 670, USA) and X-ray photoelectron spectroscopy (XPS, ESCALAB 250Xi, USA). In addition, the wettability of zinc foil in various electrolytes was assessed using a contact angle analyzer.

Electrochemical measurement

The electrochemical behavior of the Zn anode was investigated by measuring the Coulombic efficiency of Zn plating/stripping in Zn||Cu cells, the long-term reversibility of Zn deposition was examined using symmetric Zn||Zn cells. A series of electrochemical techniques was employed for comprehensive evaluation. Galvanostatic charge-discharge (GCD) measurements were carried out on a LAND CT2001 testing system to assess cycling performance under different operating conditions. Amperometric time-current responses and electrochemical impedance spectroscopy (EIS) were recorded on a CHI760 workstation, with EIS conducted over a frequency range of 0.01 to 10^5 Hz. In addition, cyclic voltammetry (CV) and Tafel analyses were performed to elucidate electrochemical reaction kinetics and interfacial mechanisms.

Theoretical calculations

Density functional theory (DFT) calculations were carried out using the CASTEP package within Materials Studio. The exchange–correlation effects were treated with the Generalized Gradient Approximation (GGA) using the Perdew–Burke–Ernzerhof (PBE) functional. A plane-wave cutoff of 310 eV was applied for the expansion of valence electron states. Interactions between ions and valence electrons were modeled using an all-electron approach. The convergence threshold for the self-consistent field (SCF) iterations was set to 1.0×10^{-6} eV per atom. To model the Zn (002) surface, a 3×3×1 supercell composed of three atomic layers and a 15 Å vacuum slab was constructed. The uppermost layer was allowed to relax, while the bottom two layers remained fixed during optimization. The adsorption energy (E_{ads}) of different functional groups on the Zn surface was determined according to:

$$E_{ads}=E_{Zn+X}-E_{Zn}-E_{X}. \qquad \text{Equation (S1)}$$

where E_{Zn+X} is the total energy of the Zn surface with the adsorbed species, E_{Zn} is the energy of the clean Zn slab, and E_X is the energy of the isolated functional group.

Calculation Methods

The ionic conductivity σ was determined according to:

$$\sigma = \frac{L}{R_b \cdot S} \qquad \text{Equation (S2)}$$

where (R_b) is the bulk resistance from EIS, (L) is the electrode separation, and (S) is the contact area.

The activation energy (E_a) for charge transfer was extracted using an Arrhenius-type expression:

$$\frac{1}{R_{ct}} = A \exp(-\frac{E_a}{RT}) \qquad \text{Equation (S3)}$$

where R_{ct} is the charge-transfer resistance, (A) the pre-exponential constant, (R) the gas constant, and (T) the absolute temperature.

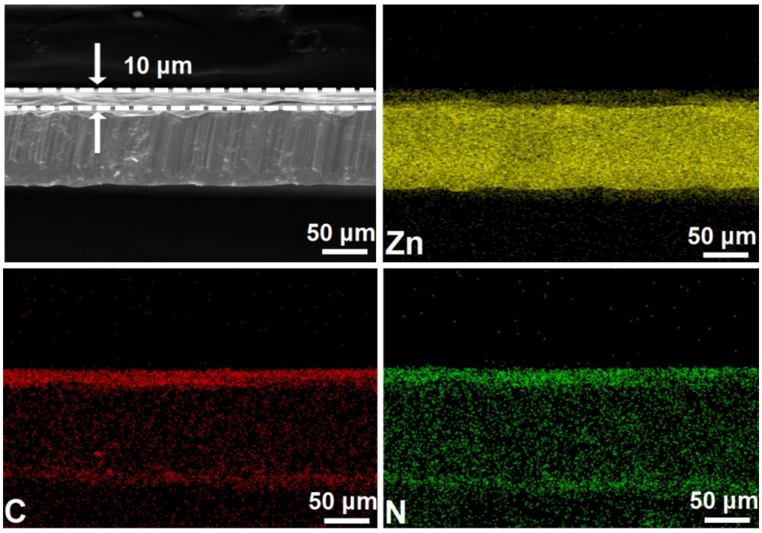

Fig. S1 Cross-sectional SEM image and EDS mapping of the PRGA@Zn electrode.

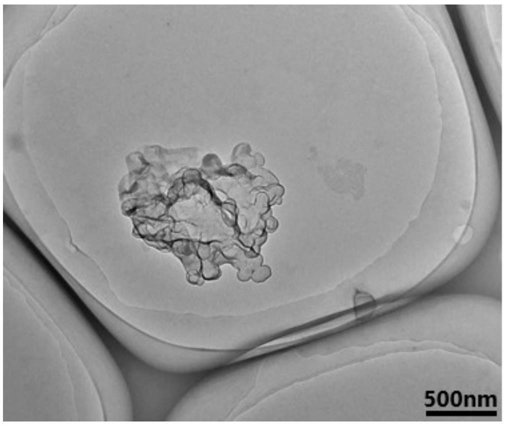

Fig. S2 The TEM image of PRGA.

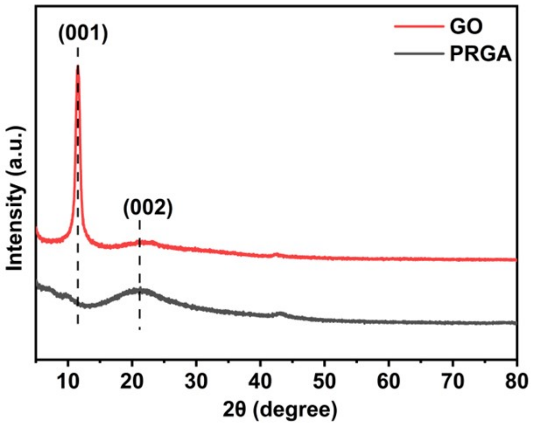

Fig. S3 XRD patterns of GO and PRGA.

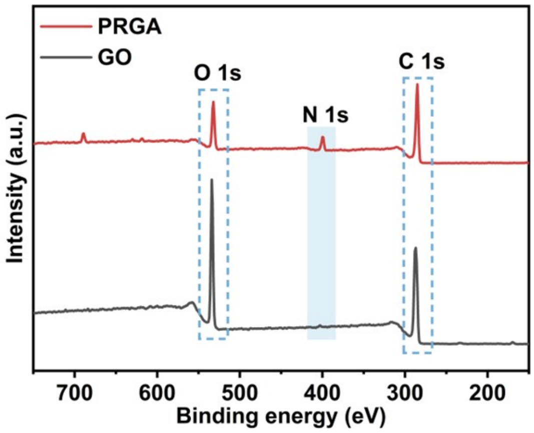

Fig. S4 The XPS spectra of GO and PRGA.

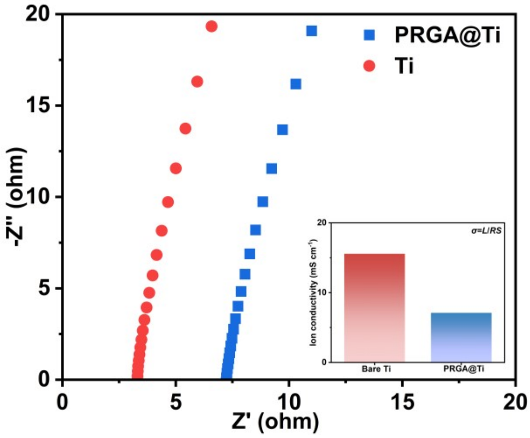

Fig. S5 Impedance diagrams of Ti foil symmetrical cells assembled with Ti and PRGA@Ti.

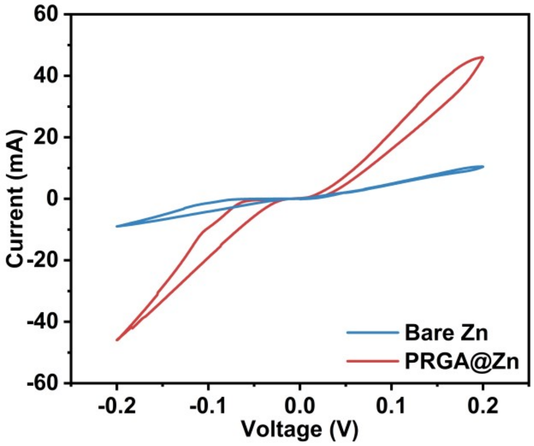

Fig. S6 CV curves of PRGA@SS||PRGA@SS and SS||SS cells at 0.1 mV s^{-1}.

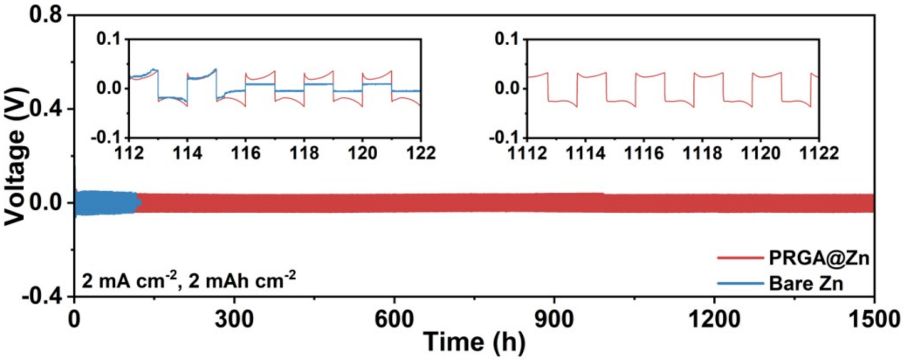

Fig. S7 The performance of the symmetrical cell with different Zn electrodes at 2 mA cm^{-2}, 2 mAh cm^{-2}.

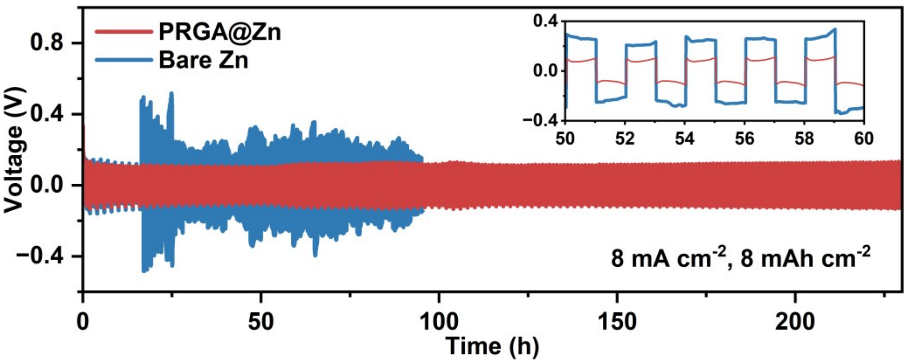

Fig. S8 The performance of the symmetrical cell with different Zn electrodes at 8 mA cm^{-2}, 8 mAh cm^{-2}.

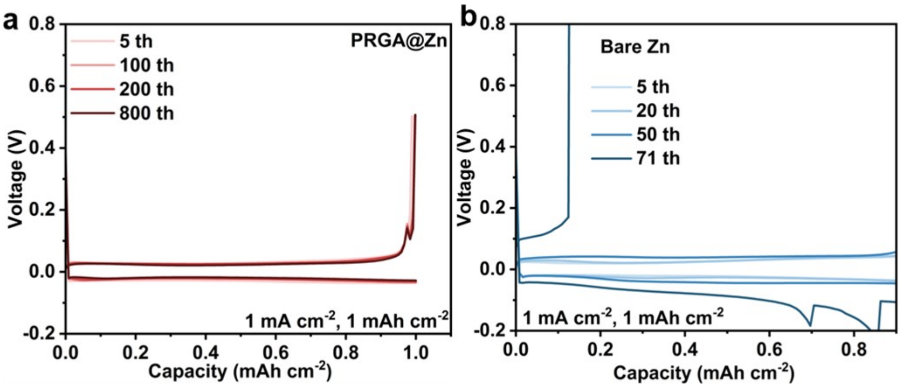

Fig. S9 The voltage-capacity curves of Zn||Cu cells based on Zn and PRGA@Zn electrode at 1 mA cm^{-2}, 1 mAh cm^{-2}.

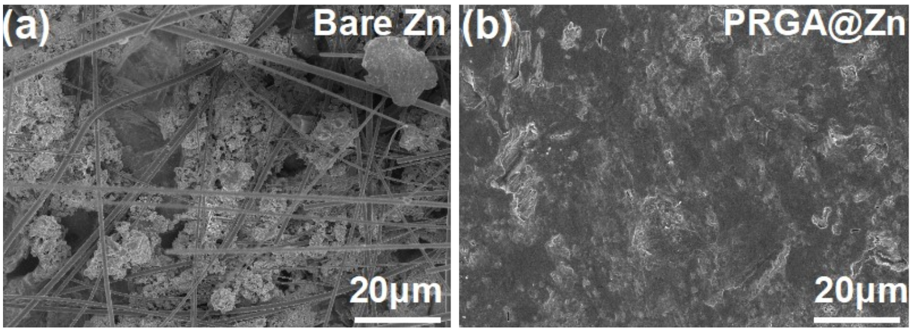

Fig. S10 SEM images of Zn electrodes after cycling in Zn||Cu cells.

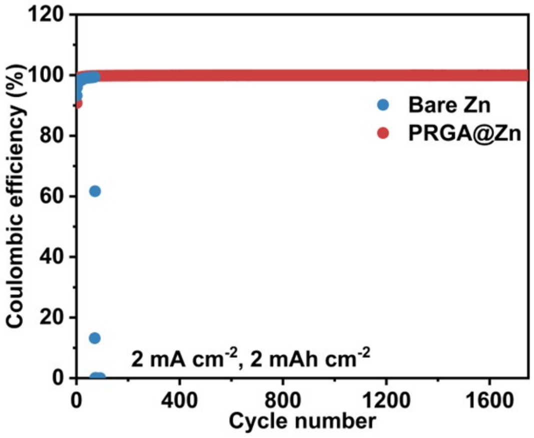

Fig. S11 CE curves of Zn||Cu asymmetric cells based on Zn and PRGA@Zn electrode at 2 mA cm^{-2}, 2 mAh cm^{-2}.

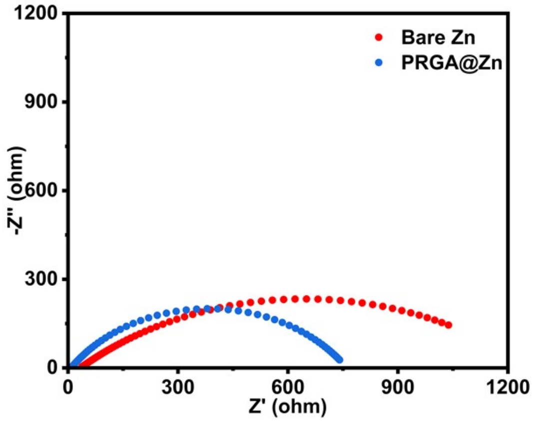

Fig. S12 EIS curves of the Zn||Zn and PRGA@Zn||PRGA@Zn cell at room temperature.

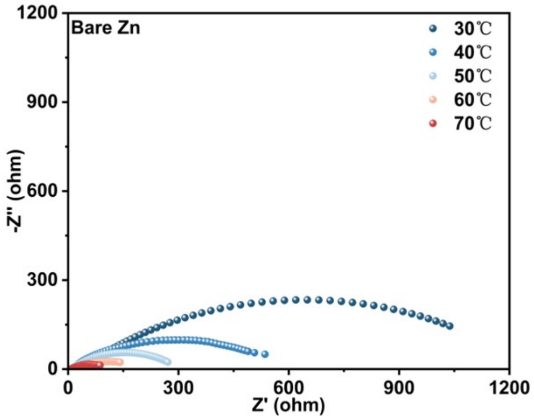

Fig. S13 EIS curves of the symmetrical cell based on the Zn electrode.

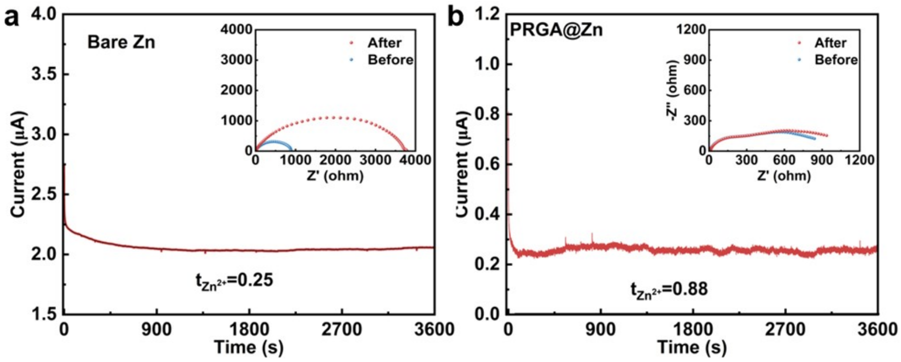

Fig. S14 Current-time curves under constant voltage polarization of 10 mV and Nyquist plots before and after polarization test for the symmetric cells based on Zn and PRGA@Zn electrodes.

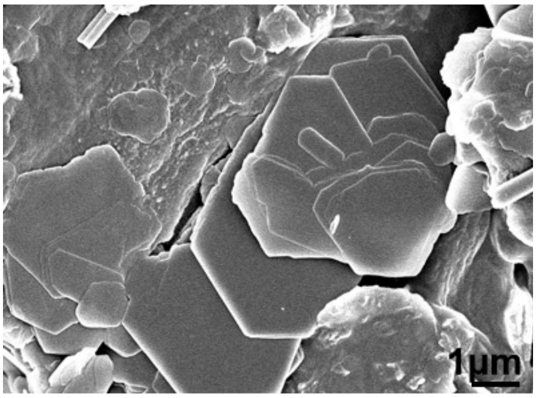

Fig. S15 SEM image of Zn electrode after cycling in Zn||Zn cells.

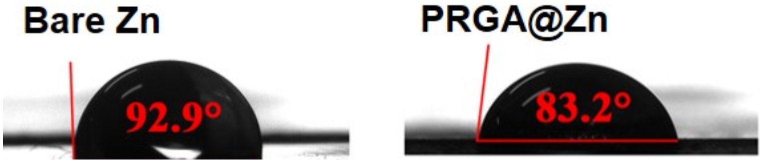

Fig. S16 Contact angle of the electrolyte on the Zn and PRGA@Zn electrode.

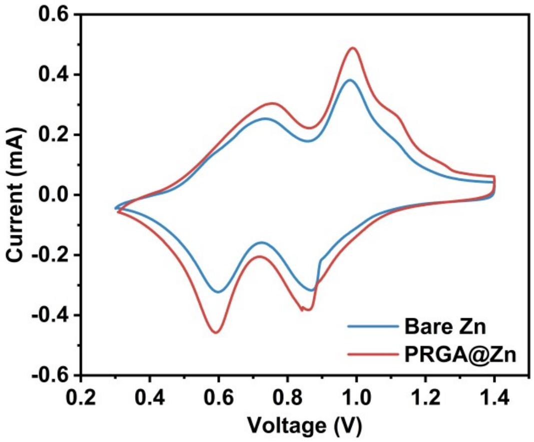

Fig. S17 CV curves of the Zn||NVO and PRGA@Zn||NVO cells at scan rates of 0.1 mV s^{-1}.

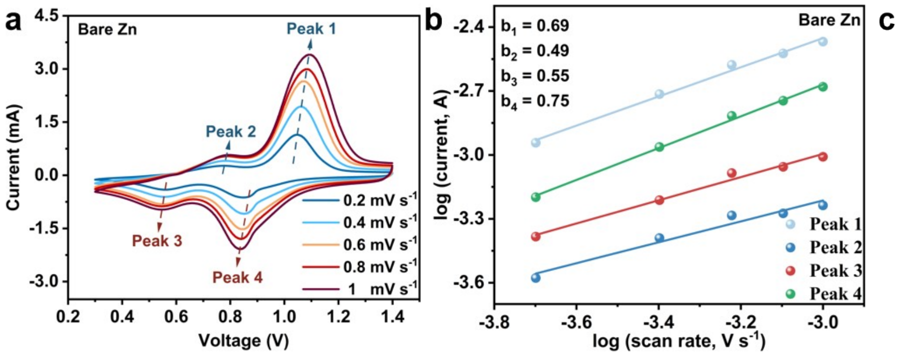

Fig. S18 (a) CV curves of Zn||NVO cell recorded at various scan rates, and (b) corresponding logarithmic plots of current versus scan rate.

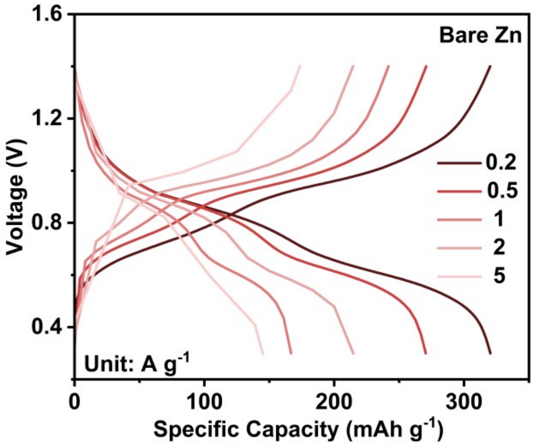

Fig. S19 Rate charge-discharge curves of Zn||NVO cell.

The PRGA@Zn‖NVO cell exhibits a substantially higher discharge capacity at a current density of 0.2 A g^{-1} compared with the Zn‖NVO cell. This improved performance originates from the PRGA@Zn anode, in which interfacial regulation induced by functional groups enables uniform Zn nucleation during the initial plating process, thereby enhancing deposition uniformity and overall electrochemical reversibility.

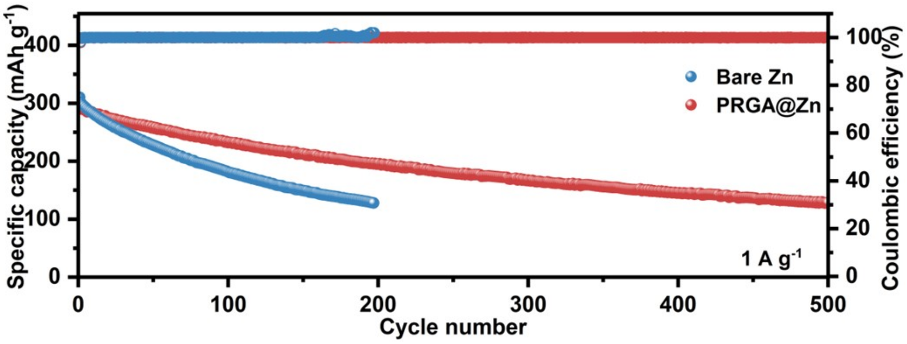

Fig. S20 Cycling stability of Zn||NVO and PRGA@Zn||NVO cells at 1 A g^{-1}.

Table S1 The R_{ct} of the cells based on PRGA@Zn||PRGA@Zn and Zn||Zn at temperatures ranging from 30°C to 70°C.

Cell	**30 ℃**	**40 ℃**	**50 ℃**	**60 ℃**	**70 ℃**
R_{ct} (PRGA@Zn||PRGA@Zn)	721	513	317	176	105
R_{ct} (Zn||Zn)	1125	582	269	195	111

Table S2 Comparison of areal capacity and lifespan with the latest reported coating strategies for stable Zn metal anodes.

Material Name	Current density ($mA\ cm^{-2}$)	Areal capacity ($mAh\ cm^{-2}$)	Cycle number	Coulombic efficiency	Reference
CZ−Zn	2	1	400	99.3 %	1
PH-CN@Zn	4	0.6	3550	99.7%	2
CZ@Zn(002)	2	2	800	99.62	3
HR–BC–Zn	1	0.5	1200	99.3%	4
Zn-ZTO	1	1	1600	99.74%	5
Zn@ZrN	1	1	270	99.5%	6
C-CNT@Zn	5	1	900	99.8%	7
AL@Zn	1	0.5	1400	99.50%	8
PRGA@Zn	**1**	**1**	**2000**	**99.89%**	**This work**
	2	**2**	**1800**	**99.90%**	**This work**

1. S. Jia, H. Bian, Q. Zhou, G. Xue, F. Li, Z. Hu, Y. Ma, J. Gu, S. Tang and X. J. N. L. Meng, *Nano Lette.*, 2025, **25**, 15651-15658.
2. J. Zhao, M. Zhang, H. Guo, X. Wang and D. J. R. M. Liu, *Rare Metals*, 2025, **44**, 6115-6124.
3. Q. Zhou, H. Bian, B. Wang, S. Jia, G. Xue, H. Wu, F. Li, Z. Hu, H. Xie, Y. Ma, J. Gu, S. Tang and X. Meng, *Chem. Eng. J.*, 2025, **504**, 159065.
4. K. Liu, Y. Li, T. Zhang, A. Zhu, G. Gan, D. Lin, K. Liu, C. Luan, S. Bu, X. Zhang, Y, Yang, Y, Wu, G. Hong and W. Zhang. *Adv. Funct. Mater.*, 2024, **34**, 2409251.
5. Y. Li, Y. H. Zhao, J. Wang, D. Xu, Y. Wang, P. Wang, Z. Liu, Q. Lai, J. Shu, Q. Zhang and T. Yi, *Adv. Funct. Mater.*, 2025, e09963.
6. X. Lu, S. Liu, L. Zhang, S. Ye, C. Yue, Y. Feng, Y. Zhou, Z. Liang, Y. Wang and W. Yang, *Small*, 2025, **21**, 2502480.
7. J. Yan, J. Qian, Y. Wang, W. Ma, Y. Chen, T. Xue, Y. Li, R. Chen and F. Wu, *Adv. Energy Mater.*, 2025, e04350.
8. C. Yang, P. Woottapanit, S. Geng, R. Chanajaree, K. Lolupiman, W. Limphirat, X. Zhang and J. Qin, *ACS Energy Lett.*, 2024, **10**, 337-344.